ELSEVIER

Numerical study of creep in two-phase aggregates with a large rheology contrast: Implications for the lower mantle

Kamel Madi [a,1], Samuel Forest [a,2], Patrick Cordier [b,*], Michel Boussuge [a,3]

[a]*Centre des Matériaux-UMR CNRS 7633, Ecole des Mines de Paris, B.P. 87, 91003 Evry, France*
[b]*Laboratoire de Structure et Propriétés de l'Etat Solide-UMR CNRS 8008 Université des Sciences et Technologies de Lille-Bat C6, 59655 Villeneuve d'Ascq Cedex, France*

Abstract

It is generally accepted that the Earth's lower mantle is dominated by two minerals, magnesiowustite (Mg, Fe)O (Mw) and (Mg, Fe)SiO$_3$ perovskite (Mg-Pv) which are thought to exhibit very different rheological properties. In order to assess the respective role of those phases in the mechanical properties of the assemblage, we have carried out 3D finite element modelling of a model two-phase aggregate. An isotropic random polycrystal has been built from a Voronoï mosaic. Then each grain has been attributed a "hard" or "weak" behavior in such a way that the hard phase represents a volume fraction of 70%. The creep law introduced for both phases is a simple power law creep without hardening. A contrast of 35 is chosen between the strain rates of both phases under a shear stress of 10 MPa. A representative volume element of 470 grains has been shown to provide a satisfactory description of the mechanical response of the aggregate with a relative precision equal to 3%. Numerical creep experiments conducted under a constant macroscopic shear stress of 10 MPa suggest that the creep rate of lower mantle assemblages would be dominated by the mechanical behavior of the harder phase (Mg-Pv). The finite element model allows one to extract the individual behavior of the two phases within the aggregate. It is shown that during creep, the harder Mg-Pv phase carries most of the stress whereas the softer Mw phase is responsible for most of the accumulated strain. This result should have implications for the development of shape and lattice preferred orientations of Mw within the aggregate, thus for seismic anisotropy of the lower mantle.
© 2005 Elsevier B.V. All rights reserved.

Keywords: plastic deformation; two-phase aggregate; MgSiO$_3$ perovskite; magnesiowustite; finite element method

---

* Corresponding author. Tel.: +33 320434341; fax: +33 320436591.

E-mail addresses: madi@mat.ensmp.fr (K. Madi), samuel.forest@ensmp.fr (S. Forest), patrick.cordier@univ-lillel.fr (P. Cordier), michel.boussuge@ensmp.fr (M. Boussuge).

[1] Tel.: +33 1 60763012; fax: +33 1 60763150.
[2] Tel.: +33 1 60763051; fax: +33 1 60763150.
[3] Tel.: +33 1 60763027; fax: +33 1 60763150.

1. Introduction

Global geodynamics is mostly due to the slow cooling of the Earth which is achieved through largescale convection of the hot mantle. Understanding the rheological properties of the Earth's interior is thus a major goal of modern geophysics. It is a formidable

challenge as the deep Earth is largely inaccessible to direct observation. Whatever the assumption made on the lower mantle bulk composition (pyrolite [1] or chondritic [2], for instance), it is likely constituted by a rock assemblage dominated by a $(Mg, Fe)SiO_3$ phase with a perovskite structure (hereafter referred to as Mg-perovskite or Mg-Pv) and by $(Mg, Fe)O$ magnesiowustite (Mw). Some minor amount of a $CaSiO_3$ perovskite phase is also likely to be present (with possibly some minor silica component: stishovite) although it will not be considered explicitly in the following. Mg-perovskite is thus by far the most important constituent with a volume fraction of the order of 70%–80%.

The contrast between the elastic properties of Mw (the softer phase; in this paper, "weak" or "soft" and "hard" or "strong" will refer to the relative strengths of the two phases at a given strain-rate and temperature) and Mg-Pv has led some authors to suggest that their plastic behavior might have a similar contrast [3]. Mw is stable under ambient pressure and appears weaker than most silicates. The rheological properties of Mg-Pv, which must be studied under extreme P, T conditions, are far less well constrained. High-pressure, room-temperature experiments have supported the hypothesis that Mw is weaker than Mg-Pv [4,5]. It is only recently that plastic deformation experiments have been carried out on Mg-Pv at high-temperature [6,7]. In situ stress measurements performed at temperatures up to 1073 K further support the idea that Mg-Pv remains the strongest phase at higher temperature [6]. It is thus commonly accepted that a representative lower mantle assemblage can be regarded, to a first approximation, as a two-phase aggregate constituted mostly by a strong Mg-Pv phase combined with 30%–40% of a much weaker Mw phase. Many authors have questioned the respective contributions of these two components to the rheology of the aggregate. Although it is often assumed that the dominant connected Mg-Pv phase should control the deformation of the assemblage (e.g. [8]), some authors suggest that the presence of a much weaker phase might have a significant effect on the rheology of the assemblage [3].

The rheology of a polyphase assemblage is complex due to stress and strain partitioning between the individual constituents. It depends on many factors including the rheology contrast between the phases,

the volume fractions and the phase distributions within the aggregate [9–14]. The rheological behavior of the polyphase aggregate is not necessarily found by averaging between the rheologies of the individual phases even when they have very comparable characteristics [15]. The simplest modelling approach consists in assuming that either strain-rate or stress is homogeneous within the aggregate, corresponding respectively to the Taylor and Reuss bounds. The actual response of any real aggregate must lie within these two rigorous upper and lower limits. For microstructures with a high contrast of properties, the Reuss and Taylor models are too far apart to give a useful estimate of the effective properties. Tharp [16] suggested that some aggregates with a strong phase forming an interconnected framework and a much weaker dispersed phase would behave like porous powder metals. More realistic information can be obtained by using the viscoplastic self-consistent (VPSC) approach in which the behavior of each grain is constrained (stress equilibrium and strain compatibility) by the aggregate as a whole represented by a homogeneous equivalent medium. This approach has been shown to provide robust solutions to the prediction of crystal preferred orientations in rocks (including polyphase aggregates [17,18]) but corresponds to a very specific morphology of the components.

A different approach is to use finite element modelling which introduces explicitly the morphology of the heterogeneous materials being considered (including phase distributions). Pioneering 2D studies have already been achieved on polymineralic assemblages showing the efficiency of the method [11]. In case of metals, Soppa et al. [19] showed a good qualitative agreement between experimental (grating technique) and 2D calculated distributions of strain fields in Ag/Ni composites. Finite element modelling is now able to predict the mechanical properties of 3D aggregates with realistic morphologies [20–24]. A further advantage is that finite element modelling also highlights the heterogeneities that develop inside the grains. John et al. [25] have deduced the intra-grain properties in a gamma titanium aliminide alloy from an integrated experimental and analytical approach. Hartig et al. [26] have investigated the effects of plastic interaction between a soft phase (copper) and a hard phase (iron) in two-

phase mixtures of ductile polycrystalline particles. The measured quantities (macroscopic stress and strain, elastic strains and texture) were compared with the results from 3D finite element calculations. Stress and strain fields were in reasonably good agreement with experiments.

The aim of the present work is to design a generic numerical experiment to address the issue of the relative importance of Mw and Mg-Pv on the rheology of their aggregate taking advantage of the recent progress of 3D finite element modelling. Our model lower mantle aggregate exhibits the most simple morphology with both phases having the same grain size and being distributed homogeneously within the aggregate. The two phases are characterized by a large rheology contrast with the hard phase occupying 70% of the volume. The creep behavior of this aggregate is calculated using the finite element method. The mechanical response of the aggregate as well as of individual phases within it are presented to answer the following questions: which phase dominates the rheology of the aggregate? How do stress and strain partition between the two phases?

2. Computational method

In contrast to the bounding or analytical estimation technique, the computational methods introduce explicitly the morphology of the random heterogeneous materials being considered [27]. They rely on solving boundary value problems on volume elements of the material. The finite element method is chosen for the computations presented in this work. A generic representation of the microstructure of random materials is chosen, namely the so-called Voronoï mosaics. The corresponding parameters used in the finite element simulations of the creep behavior of a two-phase aggregate are then identified: mesh size, constitutive equations of the constituents and boundary conditions.

2.1. Generic representation of the microstructure

Although the aim of this paper is clearly to contribute to a better understanding of the rheology of the lower mantle, the authors do not pretend to provide a realistic numerical simulation of an actual lower mantle aggregate. The reason is that too much information is lacking on lower mantle assemblages as well as on the properties of the constituent minerals. As an illustration, we have no clue as to the microstructures or grain sizes in the lower mantle. However, absolute values of grain sizes are not required here since no intrinsic length scale is introduced in the simulation. For simplicity, we have decided to start from the simplest microstructures. The Voronoï mosaic model is a good candidate since it provides a granular representation of the microstructure and since it introduces a random character in the phase distribution [28]. It is an ideal representation of isotropic random polycrystals [29,21]. The Voronoï mosaic model reproduces a random distribution of grains in space according to a Poisson process, building a Voronoï tesselation of space [29]. It is also possible to superimpose a constraint of periodicity at the boundary of the volume in the generation of the Voronoï mosaic as proposed in [30] and used in [31]. Fig. 1a shows a 3D Voronoï mosaic obtained by the algorithm proposed in [21]. Each grey scale corresponds to a different grain. The phases (hard and soft) are then distributed randomly on the various grains according to a given volume fraction, which leads to the distribution shown in Fig. 1b. As a result, both phases have the same mean grain size at the beginning of the calculation. In the present study, we have chosen a volume fraction of 70% for the hard phase (supposed to represent the Mg-Pv) and 30% for the weak phase (i.e., Mw).

Fig. 2 shows in 3D the interconnecting character of both the hard and weak phases. The 3D morphology of each phase in one configuration of the material is shown in Fig. 2a. In Fig. 2b (resp. 2c), the phase Mg-Pv (resp. Mw) only is visible. The Fig. 2d represents the ensemble of all points in phase Mw that can be connected to the bottom and top faces of the cube by lines entirely contained in the phase Mw. As a result, all isolated parts of phase Mw in Fig. 2c were removed. In this way, we say that a phase is "interconnected" if most of the phase volume (here in fact 94%) is geometrically connected to the bottom and top faces of the cube. In our simulated images of Voronoï mosaics, both phases are interconnected. This feature will play a significant role in the deformation of the aggregates.
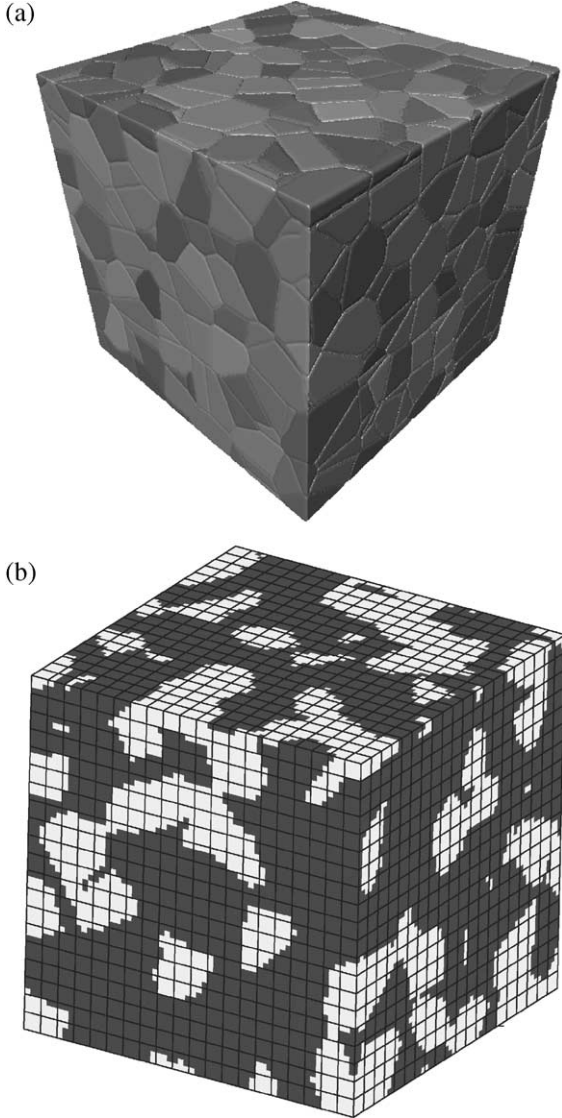
(a)

(b)

Fig. 1. (a) 3D microstructure (Voronoï mosaic containing 470 grains), (b) meshing of a two-phase material: 3D Voronoï mosaics containing 470 grains with 70% of Mg-Pv and 30% of Mw.

2.2. Properties of the constituents

The constitutive equations used for modelling the response of the phases Mg-Pv and Mw are based on a standard elastoviscoplastic framework. The total strain is decomposed into elastic and plastic parts and Hooke's law is adopted:

$$\varepsilon_{ij} = \varepsilon_{ij}^e + \varepsilon_{ij}^p, \quad \sigma_{ij} = c_{ijkl}\varepsilon_{kl}^e \tag{1}$$

The creep law introduced for both phases is a simple power law without hardening:

$$\dot{\varepsilon}_{ij}^p = \dot{p}\,\frac{3}{2}\,\frac{s_{ij}}{J_2(\sigma_{ij})}, \quad \dot{p} = \left(\frac{J_2(\sigma_{ij})}{K}\right)^n, \quad J_2(\sigma_{ij})$$
$$= \sqrt{\frac{3}{2}\,s_{ij}s_{ij}} \tag{2}$$

J_2 denotes the second invariant of the stress tensor and is also called the von Mises equivalent stress. The deviatoric part of the stress tensor is s_{ij} and p is the cumulative equivalent viscoplastic strain. The material properties of each phase are thus defined by the two parameters: K and n. As Mw is stable at ambient pressure, rheological data are available for this material (although the actual behavior under lower mantle conditions might well differ significantly from ambient pressure behavior). We have thus used existing mechanical data from [32] to determine K_w and n_w for the weak phase. More precisely, K_w was calibrated using a numerical identification method from the load-stepping tests results performed at 1400 K (from 33 MPa to 85 MPa), with increasing and then decreasing loads. These parameters are given in Table 1. The viscoplastic behavior of the hard phase is then deduced by imposing a viscosity contrast. This contrast has to be high enough for the two phases to have marked properties, but not too high, otherwise the weak phase would behave like voids. A contrast of 35 between the strain rates of both phases under a shear stress of 10 MPa represents a satisfactory compromise. No crystallographic character is introduced in the model. The local behavior of the phases is taken to be isotropic. For Mg-Pv, a stress exponent of $n=3.5$ is chosen to account for the behavior observed on analog perovskites [33,8, 34,35]. These constitutive equations are implemented in the finite element program Z-set [36]. They are integrated numerically using an implicit Newton algorithm. Note that the chosen constitutive model is very simple. In particular, the viscoplastic power law leads to a locally stable behavior. Such an approach is not able to capture strain localization phenomena like unstable shear banding or damage, in plastic materials.
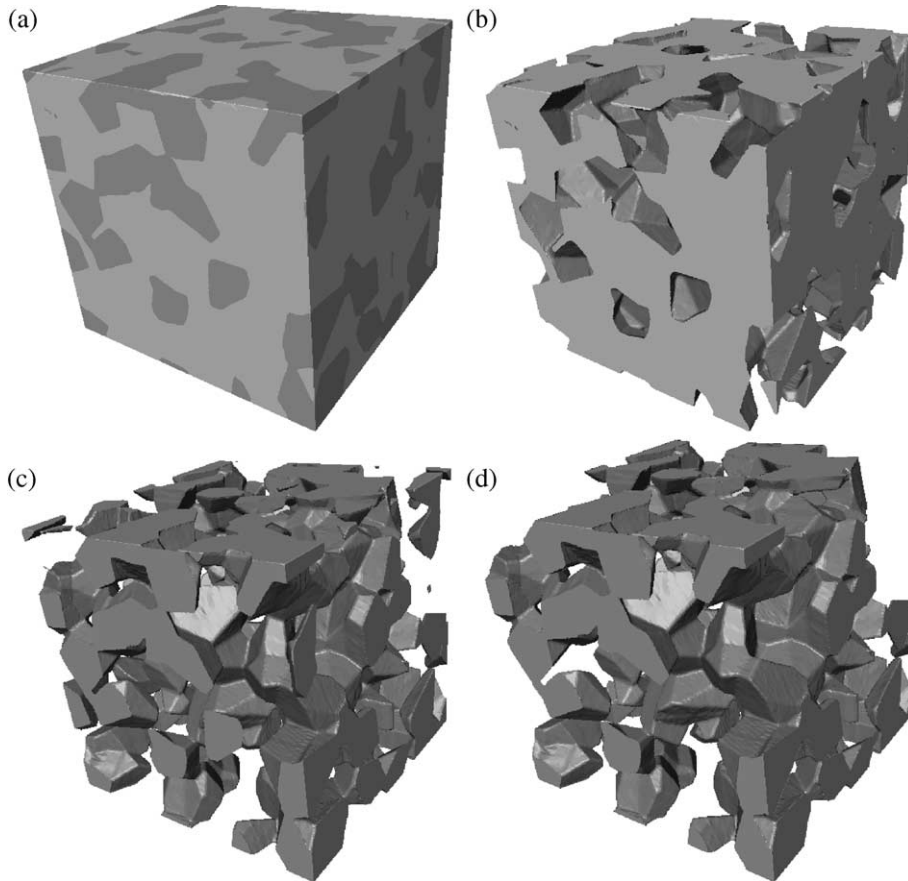
Fig. 2. (a) 3D representation of the volume (two-phase material, 470 grains), (b) 3D representation of the Mg-Pv phase inside the volume, (c) 3D representation of the Mw phase inside the volume, and (d) 3D representation of the interconnected parts of the Mw phase.

2.3. Finite element meshing

The finite element mesh associated with the image of the microstructure is obtained using the so-called multi-phase element technique [37,21]. A regular 3D finite element grid is superimposed on one image of the Voronoï mosaics. The material property is attributed to each integration point according to the color of the nearest voxel of the image. As a result, two phases may be present inside some elements. Fig. 1b shows such a mesh and the distribution of both phases. The elements are quadratic bricks (20 nodes) with complete integration (27 Gauss points).

The appropriate mesh density, defined as the average number of elements required for ensuring a given accuracy in the results of the numerical simulations, must be first determined. For that purpose, a specific microstructure made of 100 grains is used, with a volume fraction equal to 70% Mg-Pv and 30% Mw. Shear creep tests at 1400 K were simulated by applying a constant macroscopic shear stress $\sum_{12}$ equal to 10 MPa, with the boundary conditions as explained in Section 2.4. The number of cells and the geometry of the microstructure are unchanged but

Table 1
Volume fraction and mechanical data for the two phases

Phase	Volume fraction (%)	n	K (MPa$^{1/n}$)	E (GPa)	v
Mg-Pv (hard)	70	3.5	5000	441	0.25
Mw (soft)	30	4	950	307	0.25

K and n are parameters in the creep law used for the viscoplastic behavior of the two phases.

different mesh resolutions are used. The number of finite elements was changed from 100 to 8000 elements. The results given in Fig. 3 show the convergence of the macroscopic shear $\dot{E}_{12}$ of the aggregate as a function of the number of elements. A mesh density of 17 quadratic elements per grain is necessary to get a precision of 1% on the mean strain rate. We verified that this mesh density leads to a convergence of the local stress and strain fields with a precision of 5%. The largest computations presented in this work are based on a mesh containing $20 \times 20 \times 20$ elements, with 107,163 degrees of freedom and 216,000 integration points. All computations were carried out on a single workstation.

2.4. Boundary conditions

The computation cost limits the possible number of grains that can be handled in the simulation of one volume element V. In particular, such a limit size may be smaller than a so-called Representative Volume Element of the material [31]. In this case, the properties that can be computed are not necessarily the desired effective properties but merely apparent properties of the investigated volume. Kanit et al. [31] show that one can estimate the effective properties of heterogeneous materials by computing and averaging the apparent properties of a sufficient number of volumes containing a given number of grains. This statistical approach is used in the present work.

The notations used within the context of the mechanics of heterogeneous materials are the following [38]: the local strain and stress fields inside the considered volume elements are denoted by $\varepsilon_{ij}(x_k)$ and $\sigma_{ij}(x_k)$. The macroscopic strain and stress tensors are then defined as the corresponding average values over each considered volume:

$$E_{ij} = <\varepsilon_{ij}> = \frac{1}{V} \int_V \varepsilon_{ij} dV, \quad \Sigma_{ij} = <\sigma_{ij}> \tag{3}$$

In order to investigate the creep behavior of the heterogeneous material, one must be able to prescribe a given macroscopic stress tensor Σ_{ij} to each considered volume element V. For that purpose, several types of boundary conditions are available. They are listed and compared in [31]. The boundary conditions that lead to the smallest boundary layer effects and therefore to smaller representative volume elements are the periodicity conditions. The displacement field over the entire volume then reads:

$$u_i = E_{ij}x_j + v_j \quad \forall x_i \in V \tag{4}$$

where E_{ij} is the prescribed macroscopic strain tensor. The fluctuation v_i is periodic: it takes the same values at two homologous points on opposite faces. The traction vector $\sigma_{ij}n_j$ takes opposite values at two homologous points on opposite faces of V. The numerical resolution of this problem within the finite element context is such that the dual forces associated
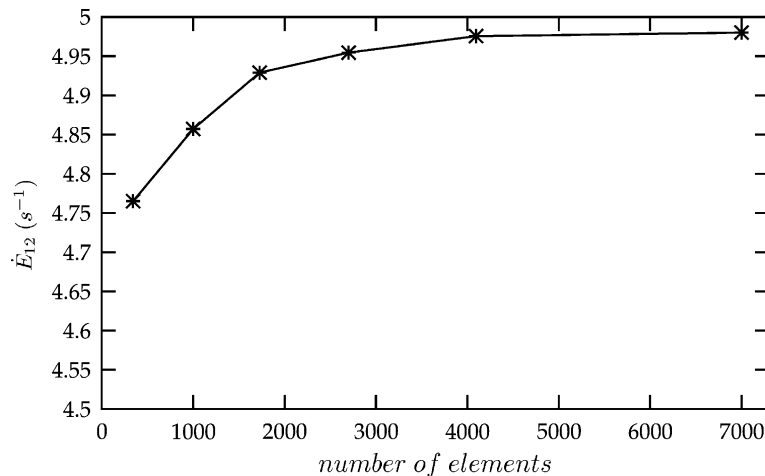

Fig. 3. Evolution of $\dot{E}_{12}$ as a function of the number of elements (3D).

to Σ_{ij} are the components of the macroscopic stress tensor E_{ij} [39]. Consequently, the periodicity conditions can be used either for prescribing mean strain or mean stress components. In the present work, all the simulations were performed by applying a constant macroscopic shear stress Σ_{12} during the creep tests, the remaining stress components being set to zero.

3. Results and discussion

In order to study local and global heterogeneities of the aggregate during a creep test, we have to consider a representative volume element of the material. The first aim of this section is to estimate the size of a representative volume element for the rock assemblage that will contain all the statistical description of the material. Then, 3D meshed representative microstructures (Fig. 1b), containing both phases (Mw (30%) and Mg-Pv (70%)) distributed among 470 grains, are deformed under creep and analysed in the Sections 3.2, 3.3 and 3.4. The creep test is simulated by applying a constant macroscopic shear stress $\Sigma_{12} = 10 MPa$ using periodic boundary conditions. First, the macroscopic response of this aggregate is studied. Second, the local behavior of the phases is analysed. Heterogeneities of stress and strain fields inside the constituent phases are analysed quantitatively. The final subsection focuses on the morphological evolution of the phases during creep in the case of large strain behavior.

3.1. Determination of the representative volume element (RVE)

In this work, the definition of the RVE is based on statistical arguments. The RVE must ensure a given accuracy of the estimated property obtained by spatial averaging of the stress, strain, or the energy fields in a given domain V. The method of determination of the size of this RVE is the following. The overall mechanical properties are studied for a large range and number of volume sizes V, given in Table 2. The convention is made that the mean volume of one Voronoï cell is 1. Accordingly, a volume contains in average $N = V$ Voronoï cells. The results are given as a function of volume V. The investigated mechanical property is the macroscopic shear strain rate $\dot{E}_{12}$ obtained for a

Table 2
Dispersion of the macroscopic shear rate as a function of the volume V

V (number of grains)	55	96	150	227	470
n (number of calculations)	120	140	89	78	25
Mean value $\bar{\bar{E}}_{12}$ $(\times 10^9 s^{-1})$	6.18	5.83	5.52	5.45	5.51
Variance $2D_{\dot{E}_{12}}$ $(\times 10^9 \ s^{-1})$	1.41	1.19	0.73	0.58	0.32
ϵ_{rel}	4.4%	4.5%	3.5%	2.9%	3.0%

prescribed stress component $\Sigma_{12} = 10 MPa$. For each calculation, the macroscopic shear rate $\dot{E}_{12}$ is then computed as the spatial average:

$$\dot{E}_{12} = <\dot{\varepsilon}_{12}> = \frac{1}{V} \int_V \dot{\varepsilon}_{12} dV \qquad (5)$$

For each volume, n different configurations of the random microstructure are simulated, containing in average $N = V$ grains. Generally, there is a dispersion of the calculated apparent strain rates for all these configurations since for each volume size the exact morphology differs from one sample to another. For larger and larger volumes the dispersion of the estimated apparent property tends to vanish. The evolution of the obtained mean value $\bar{\bar{E}}_{12}$ and variance $D_{\dot{E}_{12}}$ of the apparent macroscopic shear rate as a function of the volume size V are given in Table 2. The relative error ϵ_{rel} on the mean value is also given. In the statistical theory of samples that can be found for instance in [40,31], the absolute error ϵ_{abs} and relative error ϵ_{rel} on the mean value of a studied property Z, obtained with n independent configurations of volume V, is a function of the variance $D_z(V)$ by:

$$\epsilon_{abs} = \frac{2D_z(V)}{\sqrt{n}}, \quad \epsilon_{rel} = \frac{\epsilon_{abs}}{\bar{Z}} \qquad (6)$$

As expected, the dispersion of the results decreases when the size of the domain increases. The calculated mean values depend on the volume size and converge towards the same limit for large volumes, which can be regarded as the desired effective response of the material. The microstructure containing 470 grains is the one for which the dispersion of the results is the weakest. In this case, the relative precision on the mean value is equal to 3%. We choose this precision for the subsequent analysis of the effective material properties and the results obtained with 470 grains are

analysed systematically in the succeeding portions of the paper.

3.2. Macroscopic creep behavior of the aggregate

For a given aggregate containing 470 grains, the computed shear strain rate $\dot{E}_{12}^{FE}$ averaged over the aggregate is given in Table 3 and compared to the available analytical Taylor and Reuss models. The Taylor model assumes homogeneous strain inside the aggregate whereas the Reuss model assumes homogeneous stress. For comparison, the expected strain rates in each phase, if it were alone and submitted to the same load, are also given. These values are called $\dot{E}_{12}^{Mg-Pv\ bulk}$ and $\dot{E}_{12}^{Mw\ bulk}$, respectively. The numerical result is closer to the Taylor bound than to the Reuss bound. It can be noticed that

$$\frac{\dot{E}_{12}^{FE}}{\dot{E}_{12}^{Mg-Pv\ bulk}} = 2.3, \qquad \frac{\dot{E}_{12}^{Mw\ bulk}}{\dot{E}_{12}^{FE}} = 20 \qquad (7)$$

It turns out that the mechanical behavior of the aggregate is closer to the one of Mg-Pv than to Mw. This result is due to the fact that the Voronoï model is such that both phases are interconnected inside the volume for the given volume fractions. 3D representations of the Mg-Pv and Mw phases inside the volume are given in Fig. 2. The interconnected part of the Mg-Pv phase represents a hard skeleton which prevents unlimited deformation along the loading direction. As a result, deformation in the soft phase remains limited and does not localize into shear band for instance. The precise contributions of the individual

Table 3
Average shear strain rates $\dot{E}_{12}$ for $\sum_{12} = 10MPa$

Model	$\dot{E}_{12}$ ($\times 10^9$ s^{-1})
Bulk magnesiowustite $\dot{E}_{12}^{Mw\ bulk}$	110
Reuss approach $\dot{E}_{12}$	35
Magnesiowustite within the aggregate (FE) $\dot{E}_{12}^{Mw\ FE}$	8.7
Aggregate (FE) $\dot{E}_{12}^{FE}$	5.8
Perovskite within the aggregate (FE) $\dot{E}_{12}^{Mg-Pv\ FE}$	4.8
Taylor approach $\dot{E}_{12}$	5.0
Bulk perovskite $\dot{E}_{12}^{Mg-Pv\ bulk}$	2.5

FE stands for Finite Element simulation.

phases to the mechanical behavior of the aggregate is analysed in the next section.

3.3. Individual behavior of the two phases within the aggregate

3.3.1. Average response of the phases

The average stress and average strain of each phase in the computed aggregate are respectively denoted by $\Sigma_{12}^{Mg-Pv\ FE}, \Sigma_{12}^{Mw\ FE}, E_{12}^{Mg-Pv\ FE}, E_{12}^{Mw\ FE}$. They are plotted in Fig. 4 as a function of time. The load $\Sigma_{12} = 10MPa$ is imposed on the volume within 1 s. Two stress regimes are visible in Fig. 4a:

- The first one is a transient stage and corresponds to a redistribution of the local stresses in the phases. The instantaneous response of the phases is elastic so that both phases start with stress values close to 10 MPa at $t = 1$ s. Afterwards, the shear stress level increases significantly in the hard phase Mg-Pv and decreases in the soft phase Mw. The duration of the transient is about 3000 s for both phases.
- The second one is a steady-state creep regime characterized by a constant mean shear stress level in both phases. This asymptotic mean shear stress is found to be more than twice higher in Mg-Pv than in Mw.

The time evolution of mean shear strain components is presented in Fig. 4b. It turns out that the macroscopic shear of the aggregate is closer to the response of the Mg-Pv phase than to that of Mw. Primary creep is very short (<500 s) in Mw and secondary creep is dominant for both phases. The corresponding steady strain rate values are given in Table 3. There is a factor of 13 between the shear strain rate of Mw if it were alone and its shear strain rate $\dot{E}_{12}^{Mw\ FE}$ within the aggregate, whereas for Mg-Pv, this factor is equal to 2. Furthermore, inside the aggregate, the phase Mw deforms more than twice as fast as the phase Mg-Pv:

$$\frac{\dot{E}_{12}^{Mw\ bulk}}{\dot{E}_{12}^{Mw\ FE}} = 13, \qquad \frac{\dot{E}_{12}^{Mg-Pv\ FE}}{\dot{E}_{12}^{Mg-Pv\ bulk}} = 1.9,$$

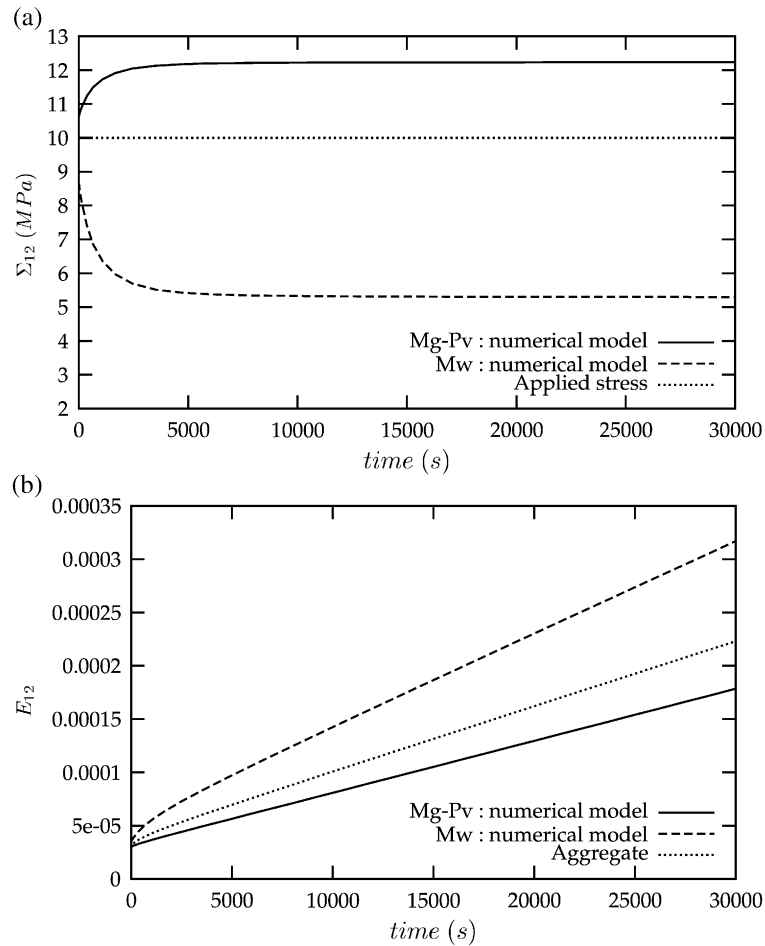$$\frac{\dot{E}_{12}^{Mw\ FE}}{\dot{E}_{12}^{Mg-Pv\ FE}} = 1.8 \qquad (8)$$

Fig. 4. (a) Applied macroscopic stress and average stress in the phases versus time, (b) macroscopic shear strain and average shear strain in the phases versus time.

As a result, it can be said that, during creep, the Mw phase is responsible for most of the accumulated strain whereas the phase Mg-Pv carries most of the stress. The main contribution of the model is to estimate the ratios of the different contributions of the phases to stress and strain.

3.3.2. Statistical analysis of intraphase fields

The Finite Element simulations provide us with a detailed description of local stress and strain inside the phases, as illustrated by the von Mises equivalent stress maps of Fig. 5 and the strain map of Fig. 6. At the beginning of the transient regime, stress is rather homogeneous in the material (Fig. 5a). The soft phase then undergoes significant stress relaxa-

tion whereas the hard phase hardens. The steady stress state is shown on Fig. 5b and can be compared with the transient one of Fig. 5a. The fact that the stress is high in almost all Mg-PV grains is related to the interconnected morphology of the phase which can carry all the load. The strain map of Fig. 6 shows that high strain is distributed over all soft grains (see Fig. 1b). This, however, cannot be interpreted as strain localization, this term being reserved to unstable behavior like in shear banding.

An important feature of the simulations is the tremendous local heterogeneities found for both stress and strain in the aggregate. Indeed, the minimum and maximum local equivalent stress/strain
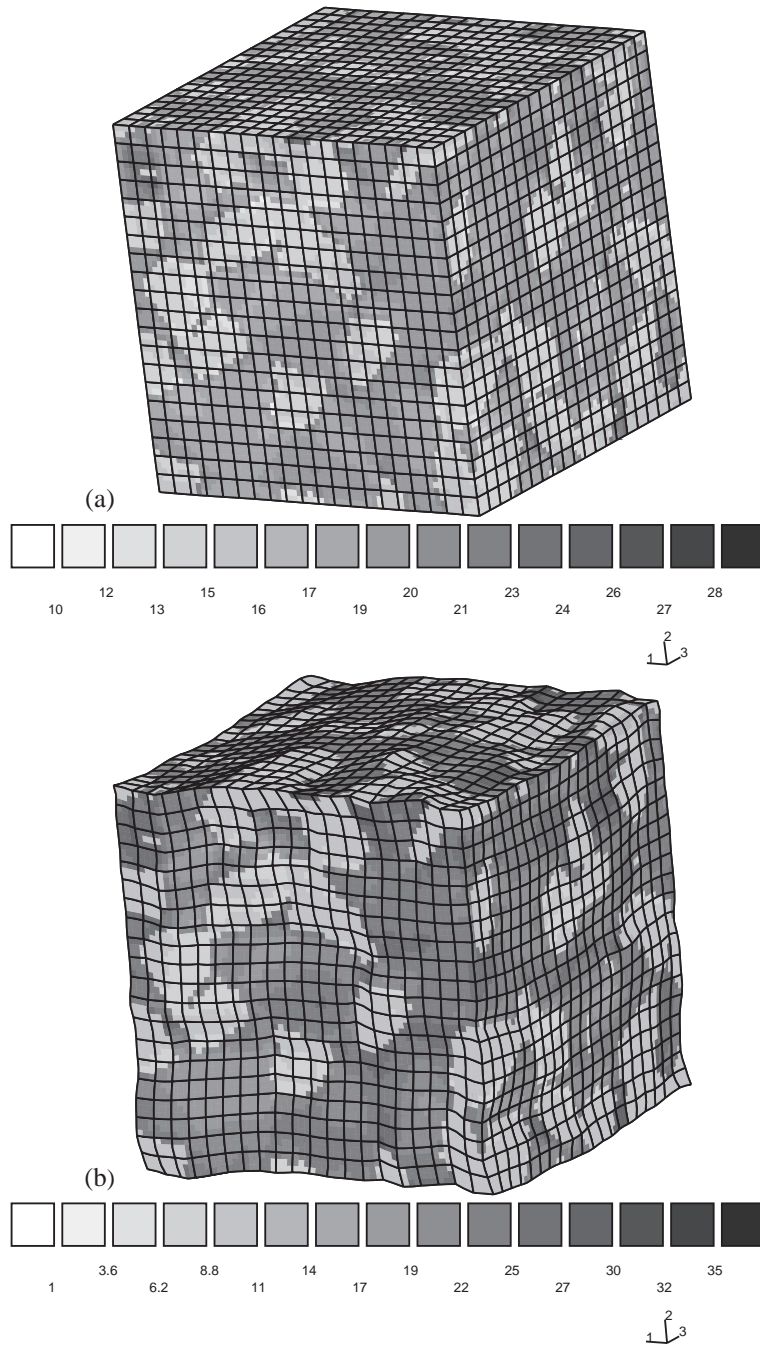
Fig. 5. Contour of von Mises equivalent stress (in MPa): (a) transient regime (at $t=400$ s), (b) steady state (at $t=30,000$ s). The macroscopic shear stress $\Sigma_{12} = 10 MPa$ was applied.

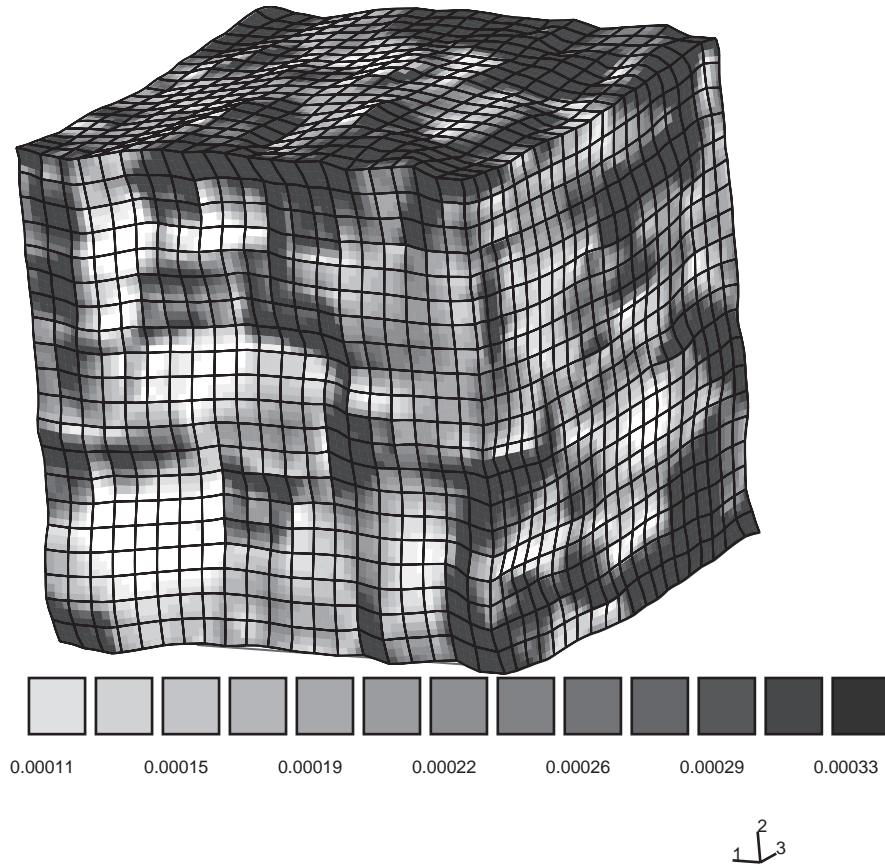Fig. 6. Contour of equivalent plastic strain p at $t = 30{,}000$ s.

values in the maps of Figs. 5 and 6 are 5.7 MPa/ 10^{-5} and 33.5 MPa/10^{-3}, respectively, for the mean prescribed shear stress/strain of 10 MPa/ 2.2×10^{-4}. This heterogeneity can be compared to that computed in the grains of a polycrystalline FCC metal in [22], where the crystallography was taken into account. In the latter reference, the polycrystal was deformed in tension at low temperature. Detailed stress and strain distributions inside individual grains can be found in [22]. In the present work, we concentrate on histograms of stress and strain that can be deduced from the simulations. The histograms for stress component σ_{12} in Mg-Pv and in Mw are given in Fig. 7a and b, respectively. They are given at different times in the transient and steady state stages. Such histograms are obtained by storing the $\sigma_{12}/\dot{\varepsilon}_{12}$ components at all integration points inside one given phase at a given time. The

studied mesh of the microstructure contains 216,000 integration points: 155,631 in the Mg-Pv phase and 60,369 in the Mw phase. These values are then ranked to construct the desired stress/strain distribution functions for each individual phase. The frequency represents the volume fraction of each phase where the local shear stress takes the value $\sigma_{12} \pm \Delta\sigma_{12}$ on the horizontal axis, where $\Delta\sigma_{12} = 0.1$ MPa is the class interval size. The corresponding histograms for the strain rate $\dot{\varepsilon}_{12}$ are presented in Fig. 8. These histograms were obtained with a class interval size of $\Delta\dot{\varepsilon}_{12} = 10^{-9}$ s^{-1}. The following statements can be made from the analysis of the calculated histograms:

• All the curves are bell-shaped, and they are symmetric with respect to the mean value, except the strain rate distributions at the beginning of the
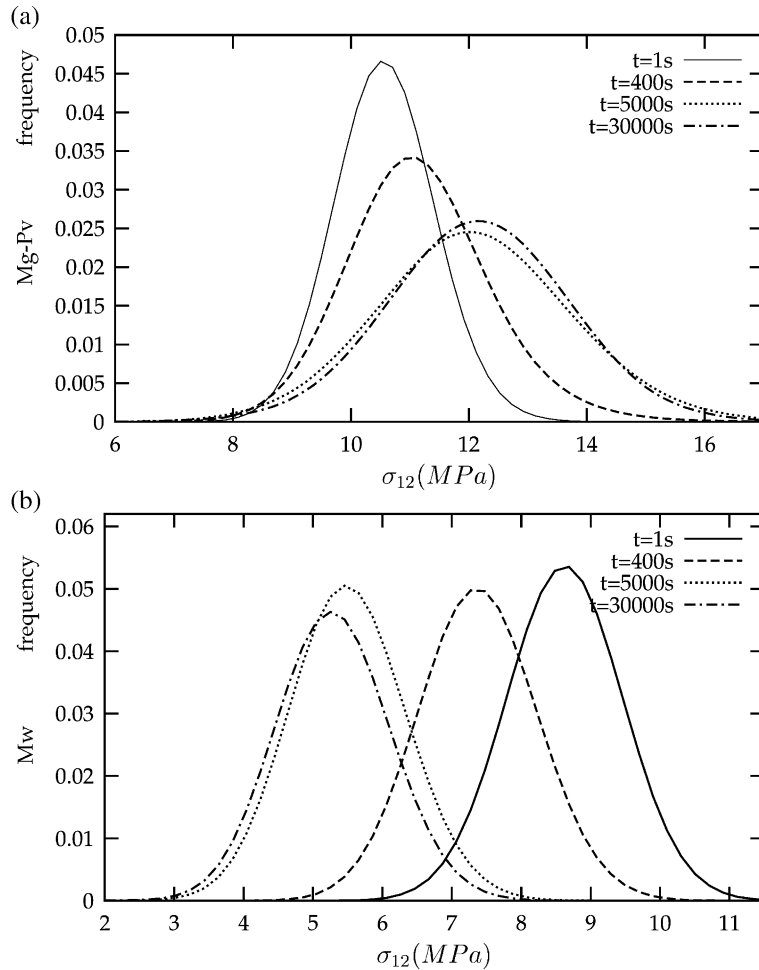
(a)

(b)

Fig. 7. Distribution of local stress versus time: (a) Mg-Pv, (b) Mw. The frequency represents the volume fraction of each phase where the local shear stress takes the value $\sigma_{12} \pm \Delta\sigma_{12}$ on the horizontal axis. These histograms were obtained with a class interval size of $\Delta\sigma_{12} = 0.1$ MPa.

transient regime (Fig. 8). Each distribution is characterized by its mean value and its standard deviation. The mean value is almost equal to the corresponding average field (shear stress or shear rate, see Table 3). The Gaussian character of the distribution was analysed using the kurtosis parameter defined as

$$k = \frac{E(x - \bar{x})^4}{\sigma^4} \quad (9)$$

where σ is the standard deviation, $\bar{x}$ is the mean of x. The kurtosis of a normal distribution is 3. The

values found for the distributions presented in this work range from 3.3 to 3.5.

- In the Mg-Pv phase, the local stress distribution progressively spreads out as a function of time and reaches a steady state distribution that changes only slightly from time $t = 5000$ s to $t = 30,000$ s. This is not the case for Mw (see Fig. 7b) where the shape of the local stress distribution remains almost invariant.
- The strain rate distribution in both phases evolves considerably from the transient to the steady state. The initial strain rate distribution is rather flat and non-symmetrical. During the transient
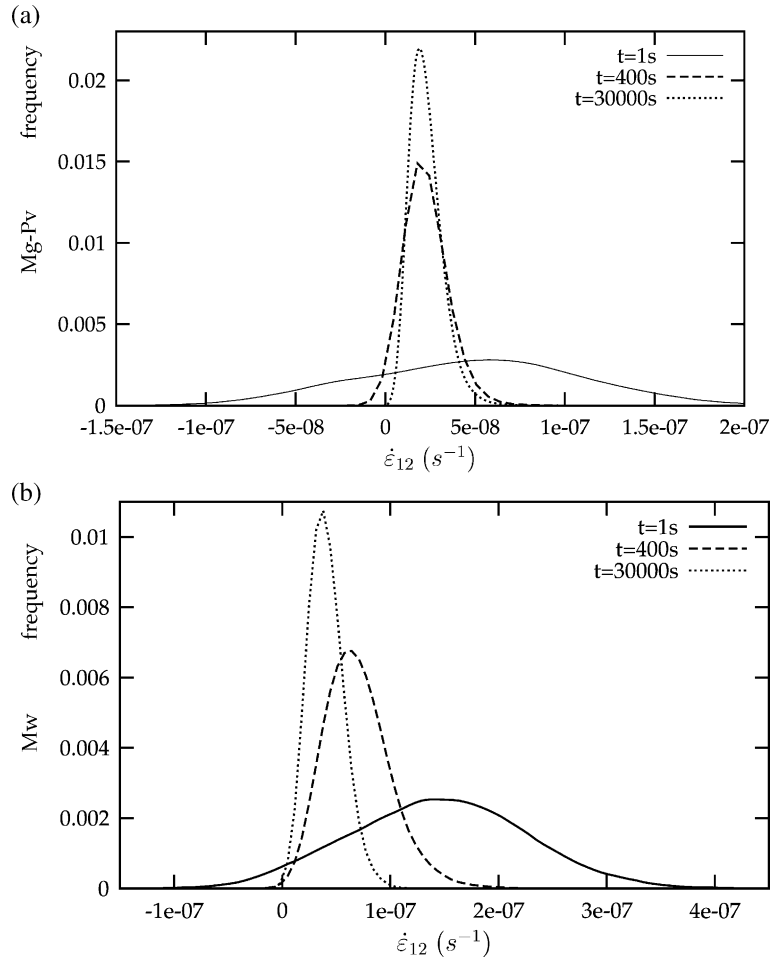
Fig. 8. Distribution of local strain-rate versus time: (a) Mg-Pv, (b) Mw. The frequency represents the volume fraction of each phase where the local shear strain rate takes the value $\dot{\varepsilon}_{12} \pm \Delta\dot{\varepsilon}_{12}$ on the horizontal axis. These histograms were obtained with a class interval size of $\Delta\dot{\varepsilon}_{12} = 10^{-9}$ s^{-1}.

regime, the mean value varies only slightly whereas the variance decreases dramatically. The initial flat distribution goes from negative to positive strain rate values as high as 2.10^{-7} s^{-1}. In contrast the final distribution lies in the positive strain rate domain.

In summary, stress tends to become more homogeneous in phase Mg-Pv than in phase Mw. This leads to a huge scatter of viscoplastic strain rates inside Mw.

We have checked that the calculated distributions do not depend on the specific morphology of a volume element containing 470 grains. Ten random-

ly generated aggregates having 470 grains and about the same volume fractions of constituents were analysed along the previous lines. The corresponding stress distributions in both phases are given in Fig. 9. The distribution functions have the same shape for all simulations. The transient regime depends on the specific morphology and shows some scatter. However, the final stress distribution is robust as it does not differ from one aggregate to the other.

Such histograms obtained experimentally based on strain field measurement methods are available in literature only for polycrystals at low temperature [41]. They confirm the bell-shaped distributions found in this work.
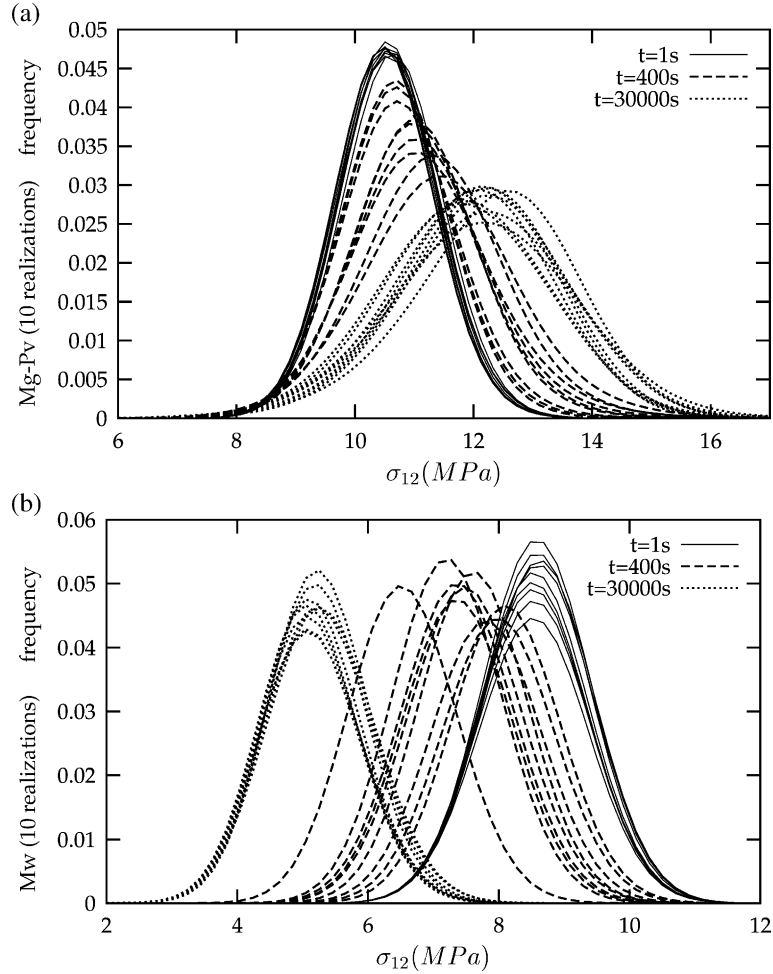
Fig. 9. Local stress distribution at different times for 10 different aggregates: (a) in the Mg-Pv phase, (b) in the Mw phase. The frequency represents the volume fraction of each phase where the local shear stress takes the value $\sigma_{12} \pm \Delta\sigma_{12}$ on the horizontal axis. These histograms were obtained with a class interval size of $\Delta\sigma_{12} = 0.1$ MPa.

3.4. Large strain behavior

Some finite element simulations of compression on the previous aggregates were also performed using a large strain formulation of the elastoviscoplastic equations. In order to reduce cost calculations, we decided to work on a microstructure containing 227 grains. Hooke's law (1) is replaced by a Jaumann rate equation for the stress [42]:

$$\sigma_{ij}^{J} = \dot{\sigma}_{ij} + \sigma_{ik}W_{kj} - W_{ik}\sigma_{kj} = c_{ijkl}D_{kl}^{e} \qquad (10)$$

The exponent J denotes the Jaumann derivative. The spin tensor W_{ij} is the anti-symmetric part of the

velocity gradient. D_{ij}^{e} is the tensor of elastic strain rate. The aim is to determine the evolution of morphology changes during compression creep starting from the previous isotropic Voronoï phase distribution. After 15% overall compression strain, local strains inside the soft phase are as high as 53%. The corresponding geometry of the phase in Fig. 10 clearly shows that the soft grains tend to deform into pancakes. Systematic analysis at larger strains is necessary to predict the final morphology of the deformed two-phase material which may well be strongly anisotropic. If such high strain morphologies can be determined, the previous analysis of
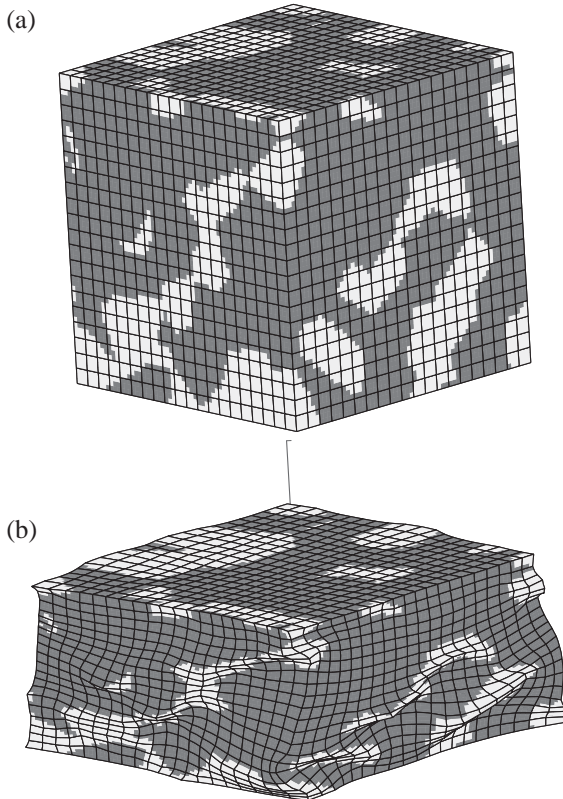
(a)

(b)

Fig. 10. Morphology changes during compression creep (overall compression strain: 15%), white color: Mw, grey color: Mg-Pv, (a) initial state, (b) deformed state.

stress/strain distribution should be performed again using more realistic microstructures than the generic one used in the present work.

4. Conclusions and prospects

This paper presents 3D simulations of creep in a two-phase aggregate, aimed at casting light on the mechanical behavior of a model lower mantle assemblage. Our goal was to perform a generic numerical experiment to assess the role of the hard (and major) and soft (and minor) phases. It appears that the rheology of the aggregate is dominated by the hard phase which forms a load-bearing framework. A consequence of the existence of a hard Mg-Pv skeleton is that the hard phase limits the overall deformation. It is interesting to note that the behavior of the aggregate is closer to the Taylor bound than to the Reuss bound.

The present study concludes that the rheology of Mg-Pv is the key parameter that controls the rheology of a lower mantle assemblage. On the other hand, most strain is produced within the weak phase (Mw). Hence, our starting microstructure (with both phases having the same morphologies and grain sizes) is not stable to high strains. Our preliminary large strain calculations suggest that Mw grains undergo significant flattening which tends to produce layering. This is an important result as shape preferred orientation can induce seismic anisotropy [43].

The question of a possible additional contribution of lattice preferred orientation to seismic anisotropy depends on the actual deformation mechanism activated into Mw (diffusion- or dislocation-creep). Without any reliable information on the grain sizes in the mantle, it is not possible so far to make any conclusion on this issue. It is also necessary in the future to incorporate additional mechanisms like grain boundary migration or dynamic recrystallization to account for the microstructure evolution in a more realistic way.

Acknowledgements

References

[1] A. Ringwood, Constitution and evolution of the mantle, Spec. Publ. - Geol. Soc. Am. 14 (1989) 457–485.

[2] D. Anderson, The earth as a planet: paradigms and paradoxes, Science 223 (1984) 347–355.

[3] S. Karato, Rheology of the lower mantle, Phys. Earth Planet. Inter. 24 (1981) 1–14.

[4] S. Merkel, H.-R. Wenk, J. Shu, G. Shen, P. Gillet, H. Mao, R. Hemley, Deformation of polycrystalline MgO at pressures of the lower mantle, J. Geophys. Res. 107 (2002) 2271.

[5] S. Merkel, H.-R. Wenk, J. Badro, G. Montagnac, P. Gillet, H. Mao, R. Hemley, Deformation of $(Mg_{0.9},Fe_{0.1})SiO_3$ perovskite aggregates up to 32 GPa, Earth Planet. Sci. Lett. 209 (2003) 351–360.

[6] J. Chen, D. Weidner, M. Vaughan, The strength of $Mg_{0.9}Fe_{0.1}SiO_3$ perovskite at high pressure and temperature, Nature 419 (2002) 824–826.

 [7] P. Cordier, T. Ungár, L. Zsoldos, G. Tichy, Dislocation creep in MgSiO$_3$ perovskite at conditions of the Earth's uppermost lower mantle, Nature 428 (2004) 837–840.

 [8] S. Beauchesne, J. Poirier, Creep of barium titanate perovskite: a contribution to a systematic approach to viscosity of the lower mantle, Phys. Earth Planet. Inter. 55 (1989) 187–199.

 [9] P. Jordan, The rheology of polymineralic rocks – an approach, Geol. Rundsch. 77 (1) (1988) 285–294.

[10] M.R. Handy, The solid-state flow of polymineralic rocks, J. Geophys. Res. 95 (B6) (1990) 8647–8661.

[11] T.E. Tullis, F.G. Horowitz, J. Tullis, Flow laws of polyphase aggregates from end-member flow laws, J. Geophys. Res. 96 (B5) (1991) 8081–8096.

[12] S. Ji, P. Zhao, Flow laws of multiphase rocks calculated from experimental data on the constituent phases, Earth Planet. Sci. Lett. 117 (1993) 181–187.

[13] P.D. Bons, J.L. Urai, Experimental deformation of two-phase rock analogues, Mater. Sci. A175 (1994) 221–229.

[14] S. Ji, B. Xia, D. Marcotte, Mechanical properties of multiphase materials and rocks: a phenomenological approach using generalized means, J. Struct. Geol. 26 (8) (2004) 1377–1390.

[15] D.F. Bruhn, D.L. Olgaard, L.N. Dell'Angelo, Evidence for enhanced deformation of two-phase rocks: experiments on the rheology of calcite–anhydrite aggregates, J. Geophys. Res. 104 (B1) (1999) 707–724.

[16] T.M. Tharp, Analogies between the high-temperature deformation of polyphase rocks and the mechanical behavior of porous powder metal, Tectonophysics 96 (1984) T1–T11.

[17] G.R. Canova, H.-R. Wenk, A. Molinari, Deformation modelling of multiphase polycrystals; case of quartz-mica aggregate, Acta Metall. Mater. 40 (7) (1991) 1519–1530.

[18] H.-R. Wenk, K. Bennett, G. Canova, A. Molinari, Modelling plastic deformation of peridotite with the self consistent theory, J. Geophys. Res. 96 (1991) 8337–8349.

[19] E. Soppa, P. Doumalin, P. Binkele, T. Wiesendanger, M. Bornert, S. Schmauder, Experimental and numerical characterisation of in-plane deformation in two-phase materials, Comput. Mater. Sci. 21 (2001) 261–275.

[20] S. Quilici, G. Cailletaud, FE simulation of macro-, meso- and micro-scales in polycrystalline plasticity, Comput. Mater. Sci. 16 (1-4) (1999) 383–390.

[21] F. Barbe, L. Decker, D. Jeulin, G. Cailletaud, Intergranular and intragranular behavior of polycrystalline aggregates: Part 1. FE model, Int. J. Plast. 17 (2001) 513–536.

[22] F. Barbe, S. Forest, G. Cailletaud, Intergranular and intragranular behavior of polycrystalline aggregates: Part 2. Results, Int. J. Plast. 17 (2001) 537–563.

[23] M. Nygards, P. Gudmundson, Three dimensional periodic Voronoi grain models and micromechanical FE-simulations of a two-phase steel, Comput. Mater. Sci. 24 (2002) 513–519.

[24] O. Diard, S. Leclercq, G. Rousselier, G. Cailletaud, Evaluation of finite element based analysis of 3D multicrystalline aggregates plasticity: application to crystal plasticity model identification and the study of stress and strain fields near grain boundaries, Int. J. Plast. 21 (4) (2005) 691–722.

[25] R. John, W.J. Porter, S. Olson, Measurement and modeling of orthotropic elastic behavior of grains in a gamma titanium aluminide alloy, Intermetallics 12 (2004) 1–9.

[26] Ch. Hartig, H. Mecking, Finite element modelling of two phase Fe–Cu polycrystals, Comput. Mater. Sci. 32 (2005) 370–377.

[27] G. Cailletaud, S. Forest, D. Jeulin, F. Feyel, I. Galliet, V. Mounoury, S. Quilici, Some elements of microstructural mechanics, Comput. Mater. Sci. 27 (2003) 351–374.

[28] S. Torquato, Random Heterogeneous Materials, Springer.

[29] E.N. Gilbert, Random subdivisions of space into crystals, Ann. Math. Stat. 33 (1962) 958–972.

[30] L. Decker, D. Jeulin, Simulation 3D de matériaux aléatoires polycristallins, Revue de Métallurgie-CIT/Science et Génie des Matériaux, 2000, pp. 271–275.

[31] T. Kanit, S. Forest, I. Galliet, V. Mounoury, D. Jeulin, Determination of the size of the representative volume element for random composites: statistical and numerical approach, Int. J. Solids Struct. 40 (2003) 3647–3679.

[32] I. Stretton, F. Heidelbach, S. Mackwell, F. Langenhorst, Dislocation creep of magnesiowüstite (Mg$_{0.8}$Fe$_{0.2}$O), Earth Planet. Sci. Lett. 194 (2001) 229–240.

[33] J. Poirier, S. Beauchesne, S. Guyot, Deformation mechanisms of crystal with perovskite structure, in: A. Navrotsky, D. Weidner (Eds.), Perovskite: A Structure of Great Interest to Geophysics and Material Science, Geophys. Monogr. Ser., vol. 16, American Geophysical Union, 1989.

[34] S. Beauchesne, J. Poirier, In search of a systematics for the viscosity of perovskite: creep of potassium tantalate and niobate, Phys. Earth Planet. Inter. 61 (1990) 182–198.

[35] Z. Wang, S. Karato, S.K. Fujino, High temperature creep of single crystal strontium titanate (SrTiO$_3$): a contribution to creep systematics in perovskite, Phys. Earth Planet. Inter. 79 (1993) 299–312.

[36] Z-set package, www.nwnumerics.com, www.mat.ensmp.fr (2001).

[37] N. Lippmann, T. Steinkopf, S. Schmauder, P. Gumbsch, 3d-finite-element-modelling of microstructures with the method of multiphase elements, Comput. Mater. Sci. 9 (1997) 28–35.

[38] P. Suquet, Continuum Micromechanics, Springer Verlag, Berlin, 1997, CISM Courses and Lectures No. 377.

[39] J. Besson, G. Cailletaud, J.-L. Chaboche, S. Forest, Mécanique Non Linéaire Des Matériaux, Hermès, France, 2001, 445 pp.

[40] E. Kreyszig, Advanced Engineering Materials, Wiley International Edition, New York, 1988.

[41] L. Allais, M. Bornert, T. Bretheau, D. Caldemaison, Experimental characterization of the local strain field in a heterogeneous elastoplastic material, Acta Metall. Mater. 42 (1994) 3865–3880.

[42] I. Doghri, Mechanics of deformable solids: linear, nonlinear, analytical and computational aspects, Springer Verlag, Berlin, 2000, 363 pp.

[43] J.P. Montagner, L. Guillot, Seismic anisotropy and global geodynamics, Plastic Deformation of Minerals and Rocks, Reviews in Mineralogy and Geochemistry, vol. 51, 2002, pp. 353–385.